Available online at www.sciencedirect.com
ScienceDirect
Solid-State Electronics 51 (2007) 1278–1286
SOLID-STATE ELECTRONICS
www.elsevier.com/locate/sse

Photonic crystal waveguide modulators for silicon photonics: Device physics and some recent progress

Wei Jiang [a,*,1], Lanlan Gu [b], Xiaonan Chen [b], Ray T. Chen [b]

[a] Omega Optics, Austin, TX 78758, United States
[b] Microelectronics Research Center and Department of Electrical and Computer Engineering, The University of Texas, Austin, TX 78758, United States

Received 5 April 2007; received in revised form 21 July 2007; accepted 3 August 2007
Available online 19 September 2007

The review of this paper was arranged by Stephen Goodnick, Anatoli Korkin, Toshio Naito and Nasser Peyghambarian

Abstract

We review the basic principles, structural designs, and electrical characteristics of photonic crystal waveguide modulators based on slow light Mach-Zehnder interferometers. A number of structural and electrical configurations of photonic crystal waveguide modulators are discussed. In addition to the advantages associated with the slow group velocity, photonic crystal waveguide modulators are found to exhibit other structural and optoelectronic merits for high speed modulation. We also briefly review past work on silicon modulators and present certain speed scaling of silicon modulators. The scaling is governed by certain intrinsic optoelectronic properties of silicon and fundamental nature of light, and plays a significant role in determining the minimum ac current density and power of silicon modulators as demonstrated in some recent experiments.

PACS: 42.70.Qs; 42.79.Hp; 42.60.Fc; 42.79.Ta; 42.82.Ds; 42.65.Re

Keywords: Photonic crystal; Silicon photonics; Modulator

1. Introduction

Silicon, the premium material for the semiconductor industry, has long been excluded from the list of favorable optoelectronic materials owing to some of its intrinsic optical properties. An indirect bandgap results in extremely low radiative recombination efficiency of silicon, which remains the main stumbling block for developing silicon lasers [1]. The intrinsic lattice symmetry prohibits silicon to have second-order optical nonlinearity, which limited the use of silicon in optoelectronic devices such as modulators and switches [2,3]. Soref and Bennett studied the effect of free carriers in silicon in 1987 [4]. They concluded that the plasma dispersion effect is adequate to produce sufficient change of refractive index with an acceptable optical loss for telecommunication wavelengths. Lorenzo and Soref subsequently demonstrated some switching effect with an integrated silicon device [5]. This opened new avenues to active photonic devices on silicon. However, for over a decade and a half, the speed of silicon modulator never reached the gigahertz mark [6–12], although gigahertz modulation was predicted in a certain resonant structure on silicon [13,14]. The turning point came in 2004 when a research group from Intel abandoned the dominant p–i–n diode configuration for silicon modulators and broke the gigahertz barrier with today's favorite structure for digital electronics: the metal–oxide–semiconductor (MOS) capacitor [15]. In the next year, Lipson's group at Cornell discovered that a p–i–n diode, when integrated into a micro-ring

* Corresponding author. Tel.: +1 512 826 4621.
E-mail address: jiang@ece.utexas.edu (W. Jiang).
[1] Current: wjiangnj@ece.rutgers.edu, Electrical and Computer Engineering Dept, Rutgers University, Piscataway, NJ 08904, USA.

0038-1101/$ - see front matter © 2007 Elsevier Ltd. All rights reserved.
doi:10.1016/j.sse.2007.08.005

resonator, did have the capability of producing gigahertz modulation [16]. These two milestone works kindled a worldwide pursuit for high speed optoelectronic devices on silicon in the last few years [17–21]. Most recently, Intel reported 30 Gbit s^{-1} transmission through a p–i–n diode modulator [21].

While the speed issue was the major concern in most part of the last two decades, the large size and power consumption of silicon modulators stand out as silicon integrated optoelectronic chips approaches reality. Intel's MOS modulators and p–i–n diode modulators generally require an interaction length of a few millimeters or longer [15,21]. The ring modulator is capable of delivering high speed with a compact form factor [16]. However, the narrow optical bandwidth of a ring resonator limits its value for high speed applications. In principle, a number of ring modulators can be cascaded to achieve a larger aggregated optical bandwidth, yet the array of rings would occupy a larger area, weakening the size advantage of micro-ring modulators. It also entails engineering issues such as accurate patching in the wavelength domain and the coordination between the cascaded rings under high injection. Nonetheless, ring modulators remain attractive for applications require compactness and less broad optical bandwidth. Also, rich physics phenomena in ring resonators add strongly to their research interests.

2. Slow light effect in a photonic crystal waveguide and its application in modulators

The beginning of 21st century witnesses the pervasive presence of nanostructures and nanofabrication in science and technology. In photonics, nanostructures, particularly photonic crystals [22–42], hold the promise of achieving the same function in a significantly reduced device size with reduced power consumption (e.g. thresholdless lasers based on photonic crystal cavities [22]). Optical waveguides based on photonic crystal line defects, the so-called photonic crystal waveguides (PCWs), have demonstrated the capability of slowing down the speed of light by up to one thousand times [28,31]. Such a slow light device has a profound impact on the phase change over a segment of photonic crystal waveguide. When incorporated in silicon Mach-Zehnder modulators photonic crystal waveguides may, as first proposed by Soljacic et al. [33], significantly enhance the phase modulation efficiency and thus reduce the modulator electrode length by several orders of magnitude. A schematic of a photonic crystal waveguide modulator is depicted in Fig. 1.

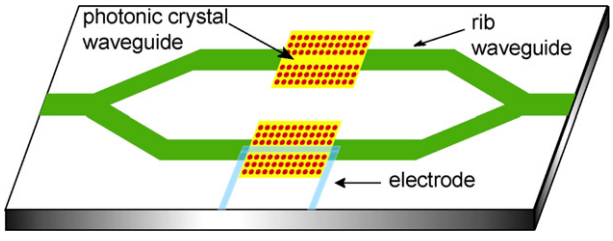

Fig. 1. A schematic of a photonic crystal waveguide modulator.

To illustrate this effect, consider a typical dispersion relation of a photonic crystal waveguide mode shown in Fig. 2a (from Ref. [36]). When the refractive index of core material changes slightly, the dispersion curve shifts vertically by an amount of $\Delta\omega_0 \sim \omega(\Delta n/n)$. Consider the effect for a fixed frequency (or, equivalently, a fixed wavelength). The change of propagation constant is related to the frequency shift through a factor inversely proportional to the group velocity,

$$\Delta\beta_{PC} = \Delta\omega_0/v_g. \tag{1}$$

The phase shift across a segment of PCW of length L can be expressed by $\Delta\phi = \Delta\beta_{PC} \cdot L$. Therefore, the interaction length required to obtain a π phase shift for a guided mode is

$$L \sim \frac{n}{2\Delta n}\frac{v_g}{c}\lambda_{air}, \tag{2}$$

where λ_{air} is the wavelength in air. Now it is evident that when the group velocity approaches zero near the band edge, the interaction length required to achieve a given phase shift can be reduced significantly.

To further understand why the change of wavevector (or propagation constant) is not simply $\Delta k = k_0\Delta n$ as in a homogeneous medium, we examine the dispersion curvature of a homogeneous medium shown in Fig. 2b. A change of refractive index causes the linear dispersion relation to change its slope, pivoting around the origin of the ω–k diagram. For a photonic crystal waveguide, the periodicity of the dispersion relation $\omega(\beta_{PC} + 2\pi/a) = \omega(\beta_{PC})$ and usual

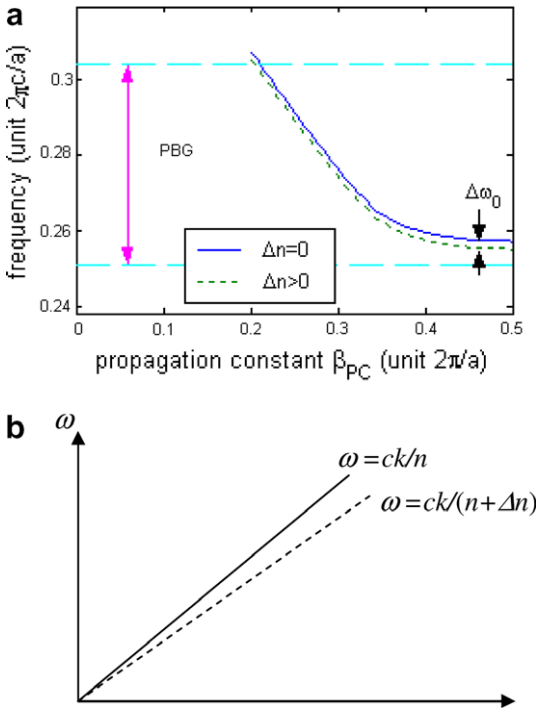

Fig. 2. (a) A typical dispersion diagram of a photonic crystal waveguide; (b) a typical dispersion diagram of a homogeneous medium.

inversion/mirror symmetry along the waveguide axis ensure an extremum (maximum or minimum) of $\omega(\beta_{PC})$ at $\beta_{PC} = \pi/a$, where $v_g = \omega(\beta_{PC}) = 0$. Upon a perturbation of the refractive index, this extremum must stay at $\beta_{PC} = \pi/a$ (we assume the lattice constant a does not change). Under such a condition, the dispersion curve only has the freedom of shifting vertically and/or changes its "effective mass" (using the terminology of the semiconductor energy bands). The change of the "effective mass" is usually negligible for a small perturbation of the refractive index. Therefore, the change of β_{PC} is mainly due to the vertical shift of the dispersion curve.

A more intuitive interpretation is that light travels slower in a PCW and has more time to interact with electrons. This results in enhanced light-matter interaction and allows for the shrinkage of the interaction length.

3. Engineering a photonic crystal waveguide modulator

While the scientific principles of a photonic crystal waveguide modulator have been known since 2002, the design and fabrication of such a modulator proved to be challenging. For a device of any use in communications, high speed modulation well beyond kilohertz is desired. Engineering such a structure requires a combination of the knowledge of the physics and engineering in photonics, electronics, and heat transfer in order to realize its advantages over conventional modulators.

For an optical modulator, the most important performance indexes are modulation depth, optical bandwidth, insertion loss, half-wave voltage V_π (usually measured at DC), electrical bandwidth, driving current or power consumption. In addition, if optical modulators are to be integrated into planar lightwave circuits that can be mass manufactured with today's VLSI technology, the modulator design must be compatible with the prevailing processing and packaging technology. In these regards, the modulator design covers much broader issues beyond the scope of this paper.

Although it is possible to fabricate a Mach-Zehnder interferometer made of photonic crystal waveguides entirely, such a structure is complicated for a number of reasons. According to the foregoing discussions, the key advantage of introducing photonic crystal waveguides into a Mach-Zehnder modulator is the reduced interaction length, i.e. the length of the waveguide segment that is subject to electrical tuning of the refractive index. As discussed in a later section, it is the interaction length, not the overall length of the MZI, that relates to other critical issues such as voltage, current, and power consumption of a silicon modulator. For initial demonstrations, it is reasonable to use a photonic crystal waveguide only for this electrically controlled segment so as to reduce the design complexity of the device. This idea seems to gain popularity in many early demonstrations [35–37].

One common concern for all photonic crystal waveguide devices is the optical loss. Early demonstrated photonic crystal waveguides suffered high propagation loss in excess of 10 dB/mm. By improving fabrication accuracy and homogeneity, passive photonic crystal waveguides were later demonstrated with low propagation loss, 1.5 dB/mm for oxide-clad ones and 0.6 dB/mm for air-clad ones [38]. These values are acceptable for many miniaturized photonic crystal waveguide devices including modulators. The short lengths (<1 mm) of photonic crystal waveguides employed in these devices result in a low value of total propagation loss around 1 dB. This is also one of the reasons why photonic crystal waveguides were not used to form the entire Mach-Zehnder interferometer in many demonstrated modulators. Direct coupling from a standard telecommunication single-mode fiber to a photonic crystal waveguide may give rise to loss as high as 30 dB due to obvious mismatch in mode profiles and effective indices. A mode converter comprising an in-plane adiabatic inverse taper and a core-elevated polymeric waveguide was realized in experiments to lower the coupling loss to 3–4 dB per coupling interface [38]. Detailed characterization of the losses of passive Mach-Zehnder interferometers was also reported [35]. These experiments indicate that with a good mode converter and careful processing, PCW Mach-Zehnder modulators may have an overall insertion loss below 6 dB. Further optimization of the coupling structure may help reduce the insertion loss to even lower level.

More critical issues of device physics arise from designing the electrical structure of the modulator. There are many schemes of injecting electrons and holes into such a photonic crystal waveguide. As previously discussed, the early work on silicon modulators highly favored the p–i–n diode configuration whereas the Intel group advanced the MOS capacitor structure. To embed an electrical structure into a photonic crystal waveguide requires thoughtful analysis. Generally, the electrical structures can be divided into two categories, vertical configurations or horizontal configurations. Here we briefly comment on two structures: a vertical MOS capacitor, and a horizontal pin diode, as depicted in Fig. 3a and b, respectively.

3.1. Vertical MOS capacitor configuration

The MOS capacitor is a unipolar device. Under accumulation conditions, the fast injection and withdraw of carriers predominates over the slow and weak carrier recombination or generation processes in silicon, thereby providing a fast mechanism for modulating the refractive index of silicon. For the vertical MOS capacitor, the key problem stems from the top electrode. To reduce the optical loss, a thick poly-Si layer must be inserted underneath the top electrode to ensure the tail of the optical mode field is weak enough when it reaches the electrode. Such a thick poly-Si layer causes a W1 waveguide [28] to have multiple modes, which is undesirable for MZI. Although it is possible in principle to reduce the waveguide width and enforce the single mode condition, this generally results in a poly-Si structure with high aspect ratio. Such a structure may cause difficulties

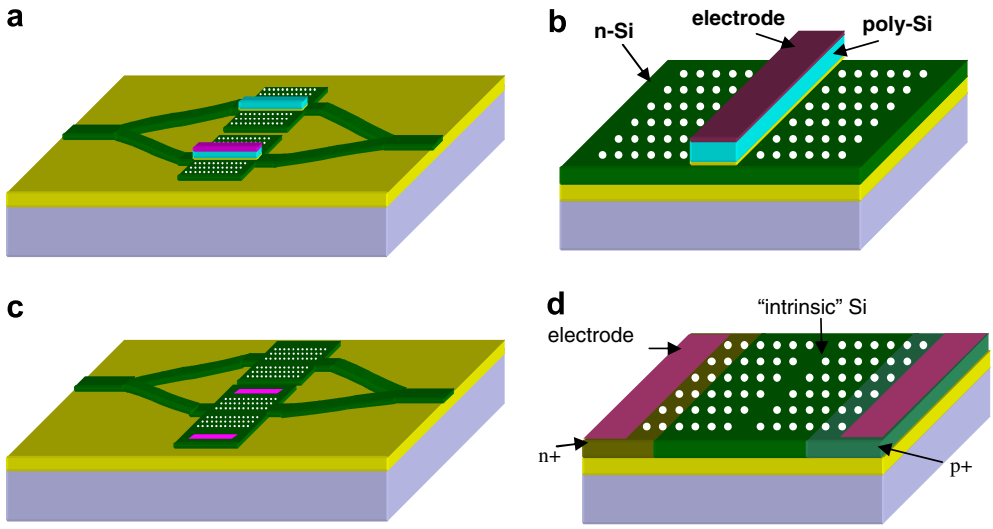

Fig. 3. Various electrical structures of a PCW Mach-Zehnder modulator: (a) & (b) vertical MOS capacitor; (c) & (d) horizontal p–i–n diode.

in planarization or other processing steps. In addition, the electric current generally flows in the electrode along the longitudinal direction, entering and exiting through the two ends of the metal wire. In such a structure, the effective crosssection for the current flow equals the waveguide width times the metal thickness. As the waveguide width is usually on the submicron scale, the crosssection is too small for a high current to pass through. Note that metal wires can sustain a current density no higher than certain limit due to the electro-migration and other issues [43]. A smaller current for such a configuration would generally result in low modulation depth. It is possible to design a complicated structure that supplies the carriers into the metal from the sides rather than the two ends. Then the effective cross-section for the electric current in the metal wire becomes equal to the waveguide length times the metal thickness, usually a two-order of magnitude increase. However, the dielectric structure of such a photonic crystal waveguide would be significantly revised from the standard type that has been well documented in literature [28,35]. Further study is needed in this area.

3.2. Horizontal p–i–n diode configurations

Horizontal configurations avoid most of the aforementioned problems associated with the vertical configurations and allow us to take advantage of the vast existing knowledge of standard photonic crystal waveguides. The MOS capacitor configuration usually gives to a thin layer of charge carriers that overlap with a very small portion of the optical mode field. This is not conducive to enhancing the interaction between light and electrons. Therefore, we considered the p–i–n diode as the first choice. The p–i–n diode based modulators were considered slower than the MOS based modulators [15]. In most silicon modulators, the carrier generation process has a negligible effect for high speed modulation. The key carrier transport/transition processes that are responsible for producing high speed optical modulation thus include carrier recombination, diffusion, and drift. For moderate to high forward injection levels, the diffusion process provides the main portion of the excess carriers and electric current. Upon a sudden switch to the reverse bias in a modulation cycle, the junction voltage and the internal field remain at relatively small values before the excess carriers stored in the i-region are removed. At this stage, diffusion and recombination are important to expedite the removal of excess carriers in the i-region. Recent simulations and experiments already revealed that the removal of carriers under reverse bias was rapid for compact p–i–n diode modulators whose waveguide cross-sections are less than 0.5×0.5 μm whereas the slow rising time under forward bias was the primary concern [12,14,16]. Finally, we would like to emphasize that a horizontal p–i–n diode is more planarized than a vertical MOS capacitor as shown in Fig. 3. The planarization advantage is of critical importance for fabrication and integration of such a modulator with microelectronic circuits, for optical interconnects and other on-chip applications.

3.3. Advantage of photonic crystal waveguides for modulators

We would like to point out another important advantage of using photonic crystal waveguides. For a modulator in the horizontal carrier injection scheme, it is desired to have a waveguide cladding that is optically insulating while being electrical conducting. In other words, light can not leak through the cladding, but electrons/holes can be injected through the cladding. A photonic crystal waveguide exactly fulfills this requirement, as shown in Fig. 4a. In contrast, in a conventional modulator, we need to etch down the side of a rib waveguide to achieve optical confinement (or making it optically insulating), as shown in Fig. 4b. This simultaneously reduces the electrical

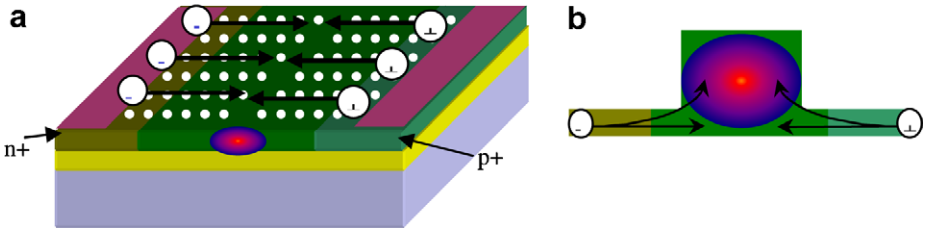

Fig. 4. Comparison of (a) a photonic crystal waveguide and (b) a conventional waveguide for optical confinement and carrier injection.

conductivity significantly, it also requires that electrons/holes to diffuse vertically to overlap with the peak of the optical field. This could significantly compromise the modulation efficiency and/or speed.

We shall mention that some early experimental work of MZIs based on photonic crystal waveguides. In 2004, a passive Mach-Zehnder interferometer (MZI) made of photonic crystal waveguides entirely was reported using compound semiconductors [32]. Subsequent work demonstrated thermo-optic tuning of the transmission by heating such a MZI [34], although it did not employ the slow light effect to reduce the switching power. Although it is possible to build a Mach-Zehnder interferometer made of photonic crystal waveguides entirely, such a structure is complicated for a number of reasons including routing the driving circuitry to the electrode between the two arms of the MZI [44].

4. Electrical characteristics of photonic crystal waveguide modulator

Although two early key demonstrations showed convincing evidence that the slow light effect did help to significantly reduce the peak switching power or current [35,36] for a photonic crystal waveguide MZI modulator, the speed of these two modulators were only suitable for certain switching/routing applications. A key issue for high speed silicon modulators is the driving voltage. Gigahertz silicon modulators typically have a peak driving voltage well above 5 V [15,16,21]. Such a high driving voltage and the accompanied high power consumption are undesirable for most on-chip applications. It turns out that the high voltage and power issues can be attributed certain intrinsic property of silicon and the fundamental limit of the size of a guided optical mode.

Intensity modulators made of silicon generally need to dynamically produce a critical carrier concentration perturbation on the order of $(\Delta N_e)_c = (\Delta N_h)_c = 3 \times 10^{17}\ \mathrm{cm}^{-3}$ [4,7,8,13]. With this general requirement, we examine the speed scaling of silicon p–i–n diode modulators. Consider an arbitrary optical waveguide whose core width is generally on the order of $w_{core} = 1\ \mu\mathrm{m}$ for wavelengths around 1.55 μm. For moderate to high forward injection, we assume that everywhere in the diode the excess carriers concentrations are non-decreasing during the forward-bias stage. Also, the carrier generation is negligible for moderate to high injection levels. Therefore, the excess carriers are ultimately supplied externally by the injected current. Regardless of the detailed carrier transport mechanism, the time required to fill the waveguide core to an optically critical level of $(\Delta N_h)_c$ in such a scenario can not be shorter than

$$\Delta t = q w_{core} (\Delta N_h)_c / J, \tag{3}$$

where J is the current density, and q is the electron charge. Note that a similar form was used to analyze a case where the recombination process prevailed [7]. Also, this limit reduces to the well-known transit time limit if the drift current dominates $J \sim q(\Delta N) v_d$, where v_d is the drift velocity.

The importance of Eq. (3) lies in the fact that the quantities q, w_{core} and $(\Delta N_h)_c$ are either fixed or have certain limits set by the fundamental physical laws. For example, the lower limit of the waveguide core width (or more accurately, the mode field width) is generally on the order of the wavelength due to the fundamental nature of light. The optically critical carrier concentration is an intrinsic property of silicon. For these reasons, this relation can be considered a fundamental limit for a wide range of silicon based intensity modulators, including the MZI, directional coupler, or other types [45].

The scaling of Eq. (3) may also be expressed in terms of the modulation frequency f. Assume the filling time takes a half period $\Delta t = 1/(2f)$, then

$$J = 2 q w_{core} (\Delta N_h)_c f, \tag{4}$$

A simple calculation shows that the scaling according to Eq. (4) requires a current density on the order of $10^4\ \mathrm{A/cm}^2$ for $f = 1$ GHz. For a conventional waveguide modulator, the cross-section for the electric current to pass is given by $A = hL$. Assuming a waveguide height h above 1 μm and a waveguide length L around 1 mm, this requires a current above 0.1 A. Note a vertical diode setting will reverse h and w_{core} but the conclusion remains the same. Even if a conventional silicon modulator can achieve a low impedance value of 50 Ω, the required power and voltage may yet not be acceptable for most on-chip optical interconnect applications [48–50]. Scaling down the device dimensions can be the answer to this difficulty. Photonic crystal based structures are capable of shrinking the device interaction length to tens of microns and the device height to hundreds of nanometers, which significantly reduces the overall current for the same current density. In some other configurations such as the vertical MOS capacitor mentioned above, the cross-section of the electric current could be $A \sim w_{core} h$.

Generally, because $w_{core} \ll L$, this significantly limits the overall current for a given maximum current density and is not desired for high speed modulators.

We shall mention that Eqs. (3) and (4) may be applicable to a MOS capacitor based silicon modulator as well. A MOS capacitor requires no electric current for dc operation. For dynamic modulation, if we assume that throughout the carrier flow path from the P^+ and N^+ contact regions to the accumulation regions near the oxide, the carrier concentrations are non-decreasing everywhere under the accumulation conditions, then again the excess carriers must be supplied by external sources. Therefore, the relation between the excess carrier concentrations and the ac current density as given in Eqs. (3) and (4) remains valid.

The electrical characteristics of the modulator were simulated using a commercial simulator Medici. Fig. 5a and b shows that for a low voltage $V_{on} = 0.89$ V, it takes a long time $\Delta t = 6.78$ ns to reach 3×10^{17} cm^{-3}, whereas for $V_{on} = 2$ V, it takes only 0.58 ns as plotted in Fig. 5c [41]. The carrier concentrations are almost independent of the depth as shown in Fig. 5a and b. Key physical processes, such as Read–Shockley–Hall recombination, Auger recombination, and impurity-concentration-dependent and field-dependent carrier mobilities, were included in our model.

The injection level $J \sim 10^4$ A/cm^2 required for gigahertz modulation falls in the high injection regime of a diode. Assume the i-region of the p–i–n diode is lightly n-doped. Under the common low injection condition where the perturbation of electron concentration $\Delta N_e \ll N_e$, we have

$$n_i^2 \exp(qV_j/k_BT) = (N_e + \Delta N_e)(N_h + \Delta N_h) \approx N_e \Delta N_h, \quad (5)$$

where n_i is the intrinsic carrier concentration of silicon, V_j the voltage across the junction, k_B the Boltzmann's constant, and T the temperature. In the high injection regime where $\Delta N_e \gg N_e$, we have [46,47]

$$n_i^2 \exp(qV_j/k_BT) = (N_e + \Delta N_e)(N_h + \Delta N_h) \approx \Delta N_e \Delta N_h. \quad (6)$$

This causes a "slower" carrier concentration increase with V_j in the form of

$$\Delta N_e = \Delta N_h = n_i \exp(qV_j/2\,k_BT). \quad (7)$$

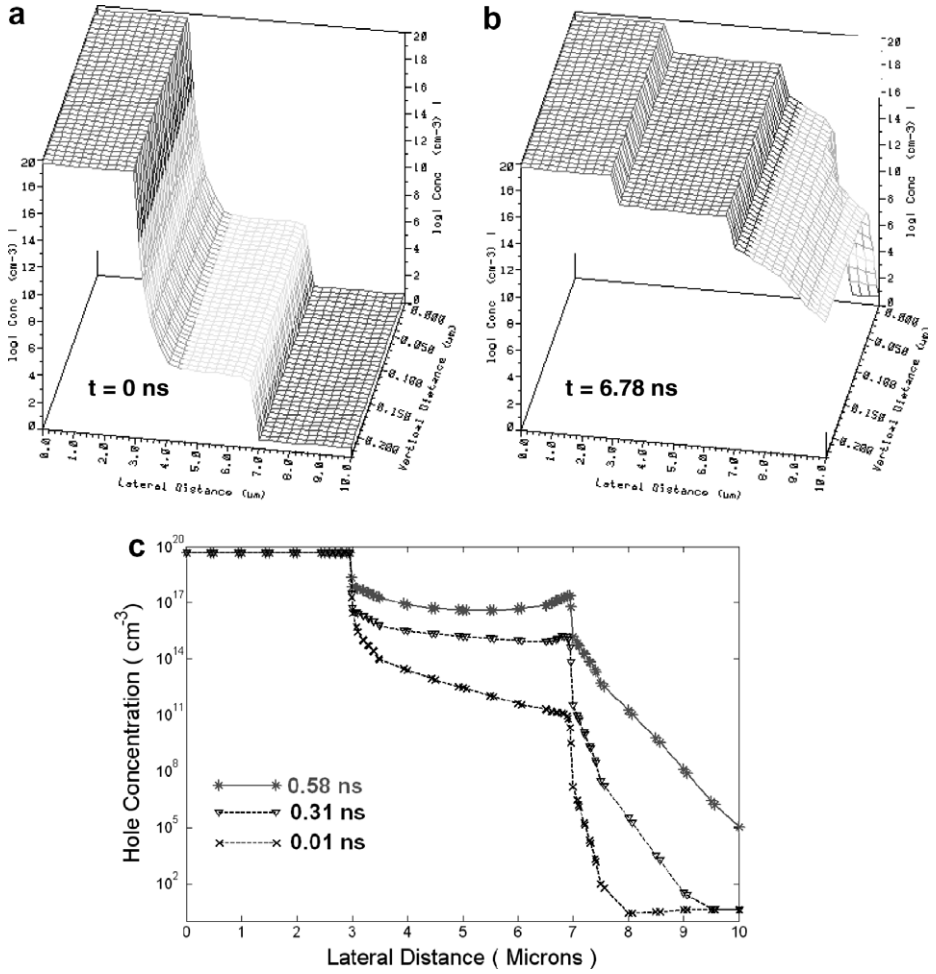

Fig. 5. Time dependent injected hole concentrations for two driving voltages. (a) and (b) 3D plot of the injected hole concentrations over the waveguide crosssection for $V_{on} = 0.89$ V. It takes a long time $\Delta t = 0.87$ s to reach the critical level of 3×10^{17} cm^{-3}. (c) 2D plot of the hole concentrations along a horizontal line at the half-depth of the top silicon layer [41].

As V_j approaches the contact potential $V_0 = (k_B T/q) \times \ln(N_a N_{di}/n_i^2)$, this gives

$$\Delta N_e = \Delta N_h = (N_a N_{di})^{1/2} \sim 2.3 \times 10^{17}\ \mathrm{cm}^{-3}, \quad (8)$$

much lower than $\Delta N_h = N_a$ for an ideal diode. Here N_a is the acceptor concentration of the p-region, and N_{di} the donor concentration of the i-region.

A simplistic estimation of voltage and power consumption is worth mentioning. Based on Eq. (4), one would obtain $I = 2$ mA for a photonic crystal waveguide having parameters $L = 80$ μm and $h = 0.25$ μm. Assume a value of the contact resistance $R_{contact} = 50\ \Omega$. The voltage drop on the contact resistance is smaller or comparable to the junction voltage. Assume an AC voltage amplitude of 1.5 V. One may estimate that the minimum power consumption would be 3 mW. For 10 GHz modulation, the current increases 10 times to 20 mA according to Eq. (4), and the voltage drop on the contact becomes substantial. Ideally, it appears possible to obtain 10GHz modulation with less than 50 mW power. However, these simplistic estimations may overlook some potential issues of actually reaching extremely high current densities [47]. We shall be wary of additional expenses we may need to pay on carrier transport for 10 GHz modulation.

5. Fabrication and measurement

Vlasov et al. fabricated a photonic crystal MZI and characterized the interference spectrum of with great care [35]. Using an unbalanced MZI that had two slightly different photonic crystal waveguides in two arms, they measured the group velocity with high accuracy and obtained an inspiring scaling of the transmission loss versus the group velocity. They also reported sub-microsecond switching time through the thermo-optic effect in such a photonic crystal MZI.

We also reported a photonic crystal waveguide modulator with an 80 micron interaction length in November 2005 [36]. Most recently, we fabricated the first *high speed* silicon photonic crystal waveguide modulator [41] on a silicon-on-insulator (SOI) wafer. The optical waveguide layer (both the conventional silicon waveguides and the photonic crystal waveguides) was patterned by electron-beam lithography and drying etching. A thin thermal oxide layer was grown to passivate the silicon surface. P^+ and N^+ regions were defined using photolithography and implanted to a concentration about $N_a = N_d = 5 \times 10^{19}\ \mathrm{cm}^{-3}$. The intrinsic region was n-doped to $N_{di} \sim 10^{15}\ \mathrm{cm}^{-3}$. The aluminum electrodes were patterned by photolithography. To sustain high current density, care was taken to design the geometry of the highly doped regions and electrodes.

The optical characterization of a high speed p–i–n diode based MZI modulator recently made by us was conducted for the transverse electric (TE) polarization at a wavelength of 1541 nm [41]. Polarization maintaining (PM) fibers with lensed taper-ends were used to couple light into the waveguides. As shown in Fig. 6a, a maximum modulation depth

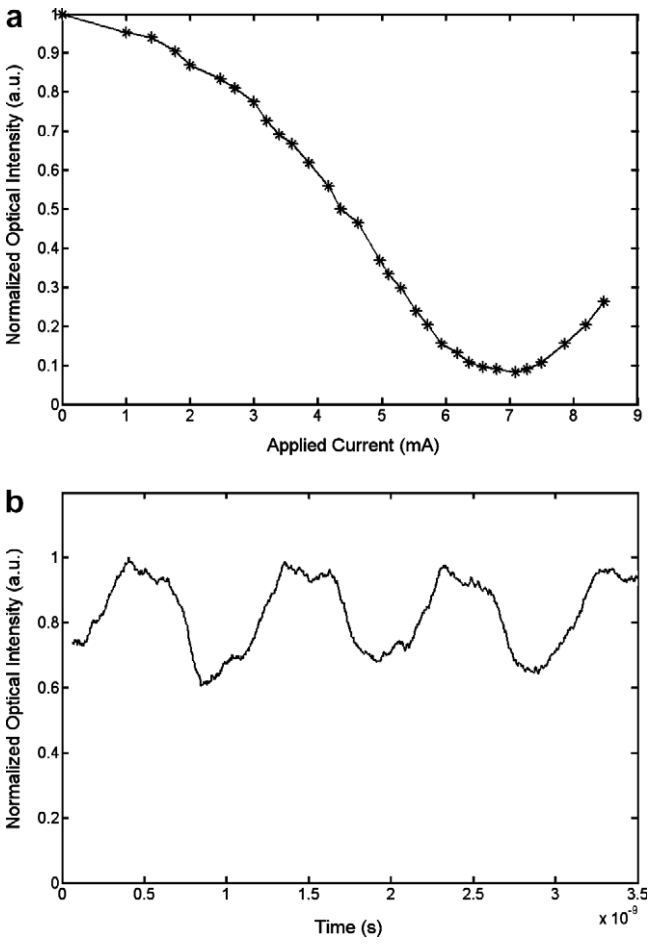

Fig. 6. Performance of a high speed PCW modulator fabricated by us [41]. (a) Optical intensity at the modulator output as a function of the static applied current. (b) The normalized output optical intensities of the modulator at 1 Gbit s^{-1}. Note the time axis has a factor of 10^{-9}.

of 93% was obtained at a static injection current of 7.1 mA, indicative of low optical absorption under an injection level around 4×10^4 A/cm^2. Square wave input electrical signals having a peak-to-peak amplitude of 3 V ($V_{on} = 2$ V, $V_{off} = -1$ V) and a duty cycle of 50% were produced by an Agilent 8133 A pulse generator. The output optical intensities of the modulator at the bit rates of 2 Mbit s^{-1} and 1 Gbit s^{-1} were measured. Thermo-optic modulation at these high frequencies is estimated to be insignificant compared to electro-optic modulation. A high modulation depth of 85% at 2 Mbit s^{-1} was obtained. The modulation depth was reduced by 3 dB as the modulation frequency increases to 1 Gbit s^{-1}, which marks the 3-dB bandwidth of our device.

Thermo-optic effects in a photonic crystal waveguide MZI have been discussed in the literature [34,35,37,42]. For a silicon modulator, it is often important to obtain a rough estimate of the thermo-optic effect against the modulation due to the plasma dispersion effect. Past work in silicon modulators investigated the static heat transfer process to give such an estimate [9,11]. Further study is necessary in this area.

Finally, a modulator entirely made of photonic crystal waveguides may be desired for further miniaturization. Many design, fabrication, and reliability issues not present thus far could emerge. For example, one shall pay attention of potential mismatch of the transmission band of the photonic crystal waveguide bends and that of a straight photonic crystal waveguide [51]. Yet no fundamental hurdle is in sight to making such a compact, low-power photonic crystal waveguide modulator that can outperform the conventional modulators in size and power with acceptable optical loss and bandwidth. With silicon CMOS technology, silicon photonic crystal guided-wave modulators may eventually reach a level of maturity ready for real world applications.

This work is supported by Air Force Office of Scientific Research.

References

[1] Pavesi L, Gaponenko S, editors. Towards the first silicon laser (NATO Science Series). Dordrecht: Kluwer; 2003.
[2] Reed GT, Knights AP. Silicon photonics: an introduction. Chichester: John Wiley; 2004.
[3] Pavesi L, Lockwood DJ, editors. Silicon photonics. Berlin: Springer; 2004.
[4] Soref RA, Bennett BR. Electrooptical effects in silicon. IEEE J Quantum Electron 1987;23:123–9.
[5] Lorenzo JP, Soref RA. 1.3 μm electro-optic silicon switch. Appl Phys Lett 1987;51:6–8.
[6] Hemenway BR, Solgaard O, Bloom DM. All-silicon integrated optical modulator for 1.3 μm fiber-optic interconnects. Appl Phys Lett 1989;55:349–50.
[7] Treyz GV, May PG, Halbout J. Silicon Mach-Zehnder waveguide interferometers based on the plasma dispersion effect. Appl Phys Lett 1991;59:771–3.
[8] Zhao CZ, Li GZ, Liu EK, Gao Y, Liu XD. Silicon on insulator Mach-Zehnder waveguide interferometers operating at 1.3 μm. Appl Phys Lett 1995;67:2448–50.
[9] Tang CK, Reed GT. Highly efficient optical phase modulator in SOI waveguides. Electron Lett 1995;31:451–2.
[10] Cutolo A, Iodice M, Irace A, Spirito P, Zeni L. An electrically controlled Bragg reflector integrated in a rib silicon on insulator waveguide. Appl Phys Lett 1997;71:199–201.
[11] Dainesi P, Kung A, Chabloz M, Lagos A, Fluckiger P, Ionescu A, et al. CMOS compatible fully integrated Mach-Zehnder Interferometer in SOI Technology. IEEE Photon Technol Lett 2000;12:660–2.
[12] Barrios AA, Almeida VR, Lipson M. Low-power-consumption short-length and high-modulation-depth silicon electrooptic modulator. J Lightwave Technol 2003;21:1089–98.
[13] Irace A, Breglio G, Cutolo A. All-silicon optoelectronic modulator with 1 GHz switching capability. Electron Lett 2003;39:232.
[14] Barrios CA, Almeida VR, Panepucci RR, Lipson M. Electro-opticmodulation of silicon-on-insulator submicron-size waveguide devices. IEEE J Lightwave Technol 2003;21:2332.
[15] Liu A, Jones R, Liao L, Samara-Rubio D, Rubin D, Cohen O, et al. A high-speed silicon optical modulator based on a metal-oxide-semiconductor capacitor. Nature 2004;427:615–8.
[16] Xu Q, Schmidt B, Pradhan S, Lipson M. Micrometre-scale silicon electro-optic modulator. Nature 2005;435:325–7.
[17] Sciuto A, Libertino S, Coffa S, Coppola G. Miniaturizable Si-based electro-optical modulator working at 1.5 μm. Appl Phys Lett 2005;86:201115.
[18] Kuo YH, Lee YK, Ge K, Ren S, Roth JE, Kamins TI, et al. Strong quantum-confined Stark effect in germanium quantum-well structures on silicon. Nature 2005;437:1334–6.
[19] Liao L, Samara-Rubio D, Morse M, Liu A, Hodge H, Rubin D, et al. High-speed silicon Mach-Zehnder modulator. Opt Express 2005;13:3129–35.
[20] Gan F, Kartner FX. High-speed silicon electrooptic modulator design. IEEE Photon Technol Lett 2005;17:1007–9.
[21] Liu A, Liao L, Rubin D, Nguyen H, Ciftcioglul B, Chetrit Y, et al. High-speed optical modulation based on carrier depletion in a silicon waveguide. Opt Express 2007;15(2):660–8.
[22] Yablonovitch E. Inhibited spontaneous emission in solid-state physics and electronics. Phys Rev Lett 1987;58:2059–62.
[23] John S. Strong localization of photons in certain disordered dielectric superlattices. Phys Rev Lett 1987;58:2486–9.
[24] Joannopoulos JD, Meade RD, Winn JN. Photonic crystals. New York: Princeton; 1995.
[25] Painter O, Lee RK, Yariv A, Scherer A, O'Brien JD, Kim I, et al. Two-dimensional photonic band-gap defect mode laser. Science 1999;284:1819–21.
[26] Ogawa S, Imada M, Yoshimoto S, Okano M, Noda S. Science 2004;305:227.
[27] Park HG, Kim SH, Kwon SH, Ju YG, Yang JK, Baek JH, et al. Electrically driven single-cell photonic crystal laser. Science 2004;305:1444–7.
[28] Notomi M, Yamada K, Shinya A, Takahashi J, Takahashi C, Yokohama I. Extremely large group-velocity dispersion of line-defect waveguides in photonic crystal slabs. Phys Rev Lett 2001;87:253902.
[29] Jiang W, Chen RT. Multichannel optical add-drop process in symmetrical waveguide-resonator systems. Phys Rev Lett 2003;91:213901.
[30] Jiang W, Chen RT, Lu X. Theory of light refraction at the surface of a photonic crystal. Phys Rev B 2005;71:245115.
[31] Gersen H, Karle TJ, Engelen RJP, Bogaerts W, Korterik JP, van Hulst NF, et al. Real-space observation of ultraslow light in photonic crystal waveguides. Phys Rev Lett 2005;94:073903.
[32] Shih MH, Kim WJ, Kuang W, Cao JR, Yukawa H, Choi SJ, et al. Two-dimensional photonic crystal Mach-Zehnder interferometers. Appl Phys Lett 2004;84:460.
[33] Soljacic M, Johnson SG, Fan S, Ibanescu M, Ippen E, Joannopoulos JD. Photonic-crystal slow-light enhancement of nonlinear phase sensitivity. J Opt Soc Am B 2002;19:2052–9.
[34] Camargo EA, Chong HMH, De La Rue RM. 2D photonic crystal thermo-optic switch based on AlGaAs/GaAs epitaxial structure. Opt Express 2004;12:588.
[35] Vlasov YA, O'Boyle M, Hamann HF, McNab SJ. Active control of slow light on a chip with photonic crystal waveguides. Nature 2005;438:65–9.
[36] Jiang Y, Jiang W, Gu L, Chen X, Chen RT. 80-Micron interaction length silicon photonic crystal waveguide modulator. Appl Phys Lett 2005;87:221105.
[37] Chu T, Yamada H, Ishida S, Arakawa Y. Thermooptic switch based on photonic-crystal line-defect waveguides. IEEE Photon Technol Lett 2005;17(10):2083–5.
[38] Notomi M, Shinya A, Mitsugi S, Kuramochi E, Ryu HY. Waveguides, resonators and their coupled elements in photonic crystal slabs. Opt Express 2004;12:1551–61.
[39] Weiss SM, Ouyang H, Zhang J, Fauchet PM. Electrical and thermal modulation of silicon photonic bandgap microcavities containing liquid crystals. Opt Express 2005;13(4):1090.
[40] Gu L, Jiang Y, Jiang W, Chen X, Chen RT. Silicon-on-insulator-based photonic-crystal Mach-Zehnder interferometers. Proc SPIE 2006;6128:261–8.
[41] Gu L, Jiang W, Chen X, Wang L, Chen RT. High-speed silicon photonic crystal waveguide modulator for low-voltage operation. Appl Phys Lett 2007;90:071105.

[42] Gu L, Jiang W, Chen X, Chen RT. Photonic crystal waveguide based silicon-on-insulator thermo-optic Mach Zehnder interferometers. IEEE Photon Technol Lett 2007;19:342.
[43] Plummer JD, Deal MD, Griffin PB. Silicon VLSI technology: fundamentals, practice, and modeling. Upper Saddle River, NJ: Prentice Hall; 2000.
[44] Jiang W, unpublished.
[45] Alferness RC. Waveguide electrooptic modulators. IEEE Trans Microwave Theory Tech 1982;30:1121–37.
[46] Streetman BG, Banerjee S. Solid state electronic devices. Upper Saddle River, NJ: Prentice Hall; 2000.
[47] Sze SM. Physics of semiconductor devices. New York: Wiley; 1981.
[48] Miller DAB. Rationale and challenges for optical interconnects to electrical chips. Proc IEEE 2000;88:728.
[49] Iqbal M, McFadden MJ, Hameed MU, Haney MW. Intrachip global interconnects and the saturation of Moore's law. In: Chen RT, editor. Technical digest of IEEE topical meeting on optical interconnects and VLSI photonics. CA, MB1.3: San Diego; 2004. p. 3–4.
[50] Chen RT, Lin L, Choi C, Liu YJ, Bihari B, Wu L, et al. Fully embedded board level guided-wave optoelctronic interconnects. Proc IEEE 2000;88:780–93.
[51] Vlasov YA. Losses in optical resonators in the slow light regime. CA: San Jose; 2006.